Laser Chem., Vol. 14, pp. 31–44
Reprints available directly from the Publisher
Photocopying permitted by license only

IDENTIFICATION OF EXCITED *GERADE* STATES OF MOLECULAR HYDROGEN WITH EXTREME ULTRAVIOLET-VISIBLE DOUBLE RESONANCE EXCITATION TECHNIQUE

JUNTAROU ISHII*, KOICHI TSUKIYAMA, and KIYOJI UEHARA*

The Institute of Physical and Chemical Research (RIKEN), Hirosawa, Wako, Saitama 351-01, JAPAN

** Department of Physics, Faculty of Science and Technology, Keio University, Hiyoshi, Kohoku-ku, Yokohama 223, JAPAN*

(Received 27 March 1993)

Extreme ultraviolet-visible double resonance excitation has been employed to populate selected rovibronic levels of the EF $^1\Sigma_g^+$, H $^1\Sigma_g^+$, I $^1\Pi_g$, and J $^1\Delta_g$ states of H_2 lying in the range between 115,000 and 117,600 cm^{-1} above the ground state X $^1\Sigma_g^+$. Tunable coherent extreme ultraviolet radiation, generated by a four-wave mixing process in Xe, prepares H_2 in the intermediate B $^1\Sigma_u^+$ (v = 6, J) state. Subsequent absorption of the visible laser radiation brings H_2 to the higher *gerade* states and the fluorescence light from these states is detected. Term values of 41 rovibronic levels in these *gerade* states, including 23 previously unidentified levels, were determined. The single rovibronic fluorescence lifetimes were also measured under the collision-free condition. The fluorescence lifetimes of the EF $^1\Sigma_g^+$ states exhibited significant rotational dependences. The nonadiabatic coupling among the adiabatic upper *gerade* vibronic states explained the observed rotational dependences successfully.

KEY WORDS: H_2, *gerade* states, fluorescence lifetimes

I INTRODUCTION

The spectroscopic study on excited *gerade* states of the hydrogen molecule which lie in the extreme ultraviolet (XUV) energy region above the ground states has a very long history. Richardson[1] and Dieke[2,3] are pioneers who set the basis of spectroscopy of the *gerade* states. They have analyzed the emission spectra of hydrogen discharges, determined rovibronic term values and other constants, and identified the perturbing interactions. However, their assignments were only partial because of the spectral irregularity caused by the vibronic mixing among the upper *gerade* manifolds.

On the other hand, the hydrogen molecule and its isotopic variants have long served as model molecular systems for theoretical treatments. Theoretical calculations on the 'double-minimum' excited states, $EF^1\Sigma_g^+$ and $GK^1\Sigma_g^+$, have been carried out by Davidson.[4,5] Dressler and co-workers[6–12] have performed *ab initio* computation based on the nonadiabatic coupling functions involving the $^1\Sigma_g^+$ (EF, GK, and H), $I^1\Pi_g^+$, and $J^1\Delta_g^+$ states, evaluating several important quantities such as energy eigenvalues and radiative lifetimes. Their calculations have resulted in a revision of previous assignments and in new identification of the strongly mixed singlet *gerade* states below the H (n = 1) + H (n = 2) dissociation limit.

A systematic measurement of the radiative lifetimes as well as the term values of various rovibronic levels in the excited *gerade* states is a useful means to verify the theoretical treatments for this simple diatomic molecule. However, these states cannot be accessed by a single dipole-allowed optical transition from the ground state $X^1\Sigma_g^+$. This difficulty has been circumvented by electron impact excitation and multiphoton or double resonance excitation. The electron impact excitation has been mainly employed for fluorescence lifetime measurements.[13–18] For example, Day et al.[15] and Sanchez and Campos[18] made use of a pulsed electron beam and measured the zero-pressure fluorescence lifetimes and the collisional quenching constants of the $GK^1\Sigma_g^+$, $I^1\Pi_g$, and $J^1\Delta_g$ states. The multiphoton or double resonance excitation with monochromatic laser light provided a quantum-state-specific detection of hydrogen molecules. The first laser-based state-selective excitation of the $^1\Sigma_g^+$ state was reported by Kligler and Rhodes.[19] Utilizing the energy coincidence between the two-photon energy of the ArF excimer laser radiation (193 nm) and the $EF^1\Sigma_g^+$ ($v' = 6$) – $X^1\Sigma_g^+$ ($v'' = 0$) transition, they determined collision-free lifetimes of the $EF^1\Sigma_g^+$ ($v' = 6$) state to be about 100 ns. Bjerre et al.[20] used an ArF excimer laser to prepare the $EF^1\Sigma_g^+$ ($v' = 6$, $J' = 0$, 1, 2) levels and a second laser to populate the states near the ionization limit. They confirmed the lifetimes reported by Kligler and Rhodes by changing the delay between the two laser pulses.

The progress in tunable coherent UV radiation sources brought a new insight on the identification of the upper $^1\Sigma_g^+$ states. From the (2 + 1) multiphoton ionization spectra taken with tunable radiation around 195 nm, Marinero et al.[21,22] carried out the first rotational analysis of the outer well of the double-minimum $EF^1\Sigma_g^+$ state. Chandler et al.[23] measured the zero-pressure lifetimes of $EF^1\Sigma_g^+$ ($v' = 0$, 3 and 6, J') of H_2, D_2, and HD by a use of a pulsed tunable UV laser in combination with a tunable near-infrared laser.

Recently a double resonance excitation technique was developed to populate single rovibronic levels of the $EF^1\Sigma_g^+$, $GK^1\Sigma_g^+$, $H^1\Sigma_g^+$, $I^1\Pi_g$, and $J^1\Delta_g$ states by our group[24,25] and to excite singlet *gerade s-* and *d- Rydberg* states near the ionization limit by Rottke and Welge.[26] In these studies, the hydrogen molecule is prepared in the selected rovibrational levels of the electronically excited $B^1\Sigma_u^+$ state with a pulsed pump beam of tunable XUV/VUV coherent radiation. The final *gerade* states are subsequently excited from the prepared levels of the $B^1\Sigma_u^+$ state with a visible/UV laser. In the present study, as an extension of our previous studies, we applied the

XUV—visible double resonance method to the $EF^1\Sigma_g^+$ ($v' = 24 \sim 29$), $H^1\Sigma_g^+$ ($v' = 1$ and 2), and $J^1\Delta_g$ ($v' = 2$) states in the range between 115,000 and 117,600 cm^{-1} where a number of rovibronic levels have still remained unidentified. By a comparison with the *ab initio* calculations, term values of 41 rovibronic levels, including 23 newly identified levels, are determined. Collision-free fluorescence lifetimes of those states are compared with the previous experimental works and the recent theoretical works by Dressler and co-workers.[6–12]

II EXPERIMENTAL

The XUV radiation used as the pump beam is generated by the resonant four-wave sum-frequency mixing using Xe gas as the nonlinear medium. Two dye lasers (Quanta Ray, PDL-2: pulse duration $\approx$ 5 ns) are pumped simultaneously by frequency doubled (532 nm) and tripled (355 nm) outputs of a Q-switch pulsed Nd:YAG laser (Quanta Ray, DCR-2A). The output of the dye laser I (Coumarin 500 or 489 in methanol) is converted into the ultraviolet (UV) radiation by a BBO crystal. The UV frequency is fixed at resonance with the two-photon transition of $6p[1/2, 0] \leftarrow {}^1S_0$ ($E = 80{,}119.474\ cm^{-1}$) of Xe. The output of the dye laser II (a 5 : 1 mixture of Rhodamine 590 and 610 in methanol) is collinearly coupled with the UV beam through a dichroic mirror. Both beams are then focused by a fused silica lens ($f = 25$ cm) into a mixing chamber in which Xe gas is provided from a valve as a pulsed jet synchronized with the laser pulses. Stainless steel parallel electrodes set at about 1 cm downstream of the valve monitors the electric current of Xe ions produced by (2 + 1) resonant-enhanced multi-photon ionization of UV photons to check the two-photon resonant condition of the UV frequency. The output energies of the dye lasers I and II are typically 5 and 2 mJ/pulse, respectively. The UV energy is estimated to be about 500 μJ/pulse. The resulting XUV radiation is introduced to a main chamber through a hole ($d = 5$ mm).

The visible probe beam is the output of a dye laser (Lumonics, Hyper Dye 300: 0.08 cm^{-1} bandwidth, pulse duration $\approx$ 10 ns) which is pumped by a XeCl excimer laser (Lumonics Pulsemaster EX-700: 308 nm output). The probe beam is collimated with a telescope and introduced into the main chamber from the opposite direction to the pump beam. In the main chamber the hydrogen gas is ejected from a pulsed valve. The tuning range between 510 nm and 580 nm is covered by Coumarin 500 and 540A dyes in methanol. The wavenumber of the probe radiation is calibrated by simultaneous recording of the I_2 excitation spectrum as a wavenumber standard.

The whole system operates with the timing pulses of 10 Hz from a function generator. The delay between the pump and probe laser pulses is controlled by a digital delay generator (Stanford Research DG535). Both laser pulses are set to overlap because the lifetime of the intermediate state is short ($\sim$ 0.8 ns). The timing of the pump and probe light pulses is monitored with a fast p-i-n photodiode (Hamamatsu S1722-02). It is necessary to readjust frequently the delay so as to compensate the long term instability of the synchronization between the YAG laser and the excimer laser.

The fluorescence light from hydrogen molecules is converged onto a photomultiplier tube by two LiF lenses. The XUV coherent radiation was tuned to the single rovibronic transition of the Lyman band system ($B^1\Sigma_u^+ \leftarrow X^1\Sigma_g^+$) by monitoring the VUV fluorescence with a solar blind photomultiplier (Hamamatsu R1459: CsI cathode). The transitions from the $B^1\Sigma_u^+$ state to the upper *gerade* states induced by the visible probe laser was then interrogated by observing the visible/near IR fluorescence corresponding to the transition between the upper *gerade* and lower *ungerade* ($B^1\Sigma_u^+$, $C^1\Pi_g$ and $B'^1\Sigma_u^+$ states) with another photomultiplier (Hamamatsu R666: GaAs cathode) through suitable optical filters (Toshiba R-64, etc.). The pulse energy is kept below ~ 300 μJ/pulse by the use of neutral density filters to avoid the saturation effect. The double resonance excitation spectrum is obtained by recording the visible/near IR fluorescence intensity as a function of the wavelength of the probe laser. For the lifetime measurement, the output is fed into a digital storage oscilloscope and then processed by a microcomputer. The measured lifetimes are dependent neither on the distance between the nozzle orifice and the probe laser beam nor on the stagnation pressure. This fact guarantees that the present experimental conditions prepare the collision-free environment. Further details of the experimental apparatus have been given in Reference 24.

III RESULTS AND DISCUSSION

III.1. Spectral assignments

A typical double resonance excitation spectrum is shown in Figure 1. The lower trace is the excitation spectrum involving the $EF^1\Sigma_g^+$ ($v' = 26$, $J' = 1$) $\leftarrow$ $B^1\Sigma_u^+$ ($v = 6$, $J = 0$) transition, whereas the upper trace represents the I_2 excitation spectrum for wavenumber calibration. At least three scans are averaged to determine the wavenumbers to the accuracy of about $\pm$ 0.05 cm^{-1}. The experimental term value, 116,031.71 cm^{-1}, of the upper level determined by summing the wavenumber of the probe laser and the known term value of the intermediate level ($B^1\Sigma_u^+$ ($v = 6$, $J = 0$))[27] agrees with a theoretical value, 116,031.65 cm^{-1}, of the *ab initio* calculation.[11] The identification of the previously unobserved states is also straightforward owing to similar good agreement between the experimental term values and the *ab initio* values. Thus, term values of 41 rotational levels in these *gerade* states, including 23 previously unidentified rovibronic levels, were newly determined. The frequencies of the probe transitions and the term values of the upper *gerade* states determined in the present work are summarized in Table I and II, respectively. The plots of the term values against J' ($J' + 1$) are illustrated in Figure 2.
Following features are worth noting:

(1) Our term values are 8.01 cm^{-1} higher than those given by Dieke[2,3], confirming the systematic error in his assignment as pointed out by Wolniewicz and Dressler.[28]

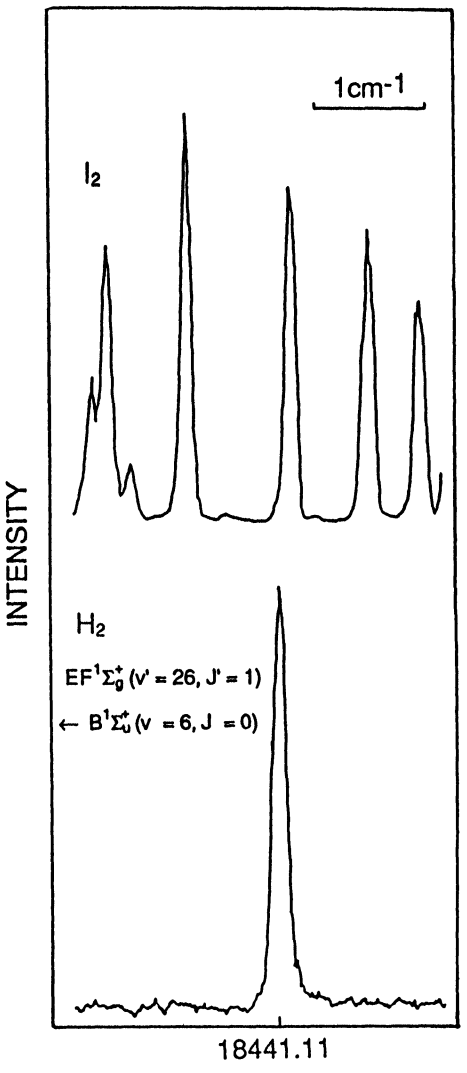

Figure 1 Double resonance excitation spectrum of H_2 involving the $EF^1\Sigma_g^+$ ($v' = 26$, $J' = 1$) ← $B^1\Sigma_u^+$ ($v = 6$, $J = 0$) probe transition (lower trace). The frequency calibration is achieved by the simultaneous recording of the I_2 $B^3\Pi(O_u^+) - X^1\Sigma_g^+$ spectrum (upper trace).

(2) The term value (116,963.16 cm^{-1}) determined for the $J^1\Delta_g^-$ ($v' = 2$, $J' = 3$) level, which agrees excellently with Dieke's value[2] after the correction of the systematic error, is 3.04 cm^{-1} higher than that for the $J^1\Delta_g^+$ ($v' = 2$, $J' = 3$) level. This inverted level structure is consistent with the *ab initio* calculation.[11]

(3) The $EF^1\Sigma_g^+$ ($v' = 26$, $J' = 0$) level is higher than $J' = 1$ level by ~10 cm^{-1}. This is also predicted by the calculation.[11]

Table 1 List of transition frequencies (cm^{-1}) between upper gerade states and the $B^1\Sigma_u^+$ (v = 6) state

$EF^1\Sigma_g^+$ (v′ = 24)	J′ = 3	←	$B^1\Sigma_u^+$ (v = 6)	J = 2	17 450.42
	2	←		3	17 309.83
	4	←		3	17 437.22
	3	←		4	17 242.59
	5	←		4	17 387.21
$EF^1\Sigma_g^+$ (v′ = 25)	J′ = 1	←		J = 0	17 987.18
	0	←		1	17 943.06
	2	←		1	17 986.05
	1	←		2	17 897.07
	3	←		2	17 973.21
	2	←		3	17 836.57
	4	←		3	17 922.76
	5	←		4	17 889.12
$EF^1\Sigma_g^+$ (v′ = 26)	J′ = 1	←		J = 0	18 441.11
	0	←		1	18 420.95
	2	←		1	18 426.70
	1	←		2	18 351.06
	3	←		2	18 407.99
	2	←		3	18 277.23
	4	←		3	18 381.46
	5	←		4	18 343.87
$EF^1\Sigma_g^+$ (v′ = 27)	J′ = 1	←		J = 0	18 932.98
	0	←		1	18 887.60
	2	←		1	18 933.89
	1	←		2	18 842.88
	3	←		2	18 923.43
	2	←		3	18 784.44
	4	←		3	18 863.39
	5	←		4	18 833.43
$EF^1\Sigma_g^+$ (v′ = 28)	J′ = 0	←		J = 1	19 294.72
	2	←		1	19 343.77
	1	←		2	19 251.18
	3	←		2	19 335.54
	2	←		3	19 194.29
	4	←		3	19 298.68
	3	←		4	19 127.69
	5	←		4	19 260.15
$EF^1\Sigma_g^+$ (v′ = 29)	J′ = 2	←		J = 1	19 770.93
	4	←		3	19 729.45
	5	←		4	19 688.39
$H^1\Sigma_g^+$ (v′ = 1)	J′ = 4	←	$B^1\Sigma_u^+$ (v = 6)	J = 3	18 007.01
	5	←		4	18 146.36
$H^1\Sigma_g^+$ (v′ = 2)	J′ = 0	←	$B^1\Sigma_u^+$ (v = 6)	J = 1	19 676.38
	1	←		2	19 657.86
$I^1\Pi_g^+$ (v′ = 2)	J′ = 2	←	$B^1\Sigma_u^+$ (v = 6)	J = 3	18 378.20

Table 1 *(Cont'd)*

$J^1\Pi_g^+$ (v' = 2)	J' = 2	←	$B^1\Sigma_u^+$ (v = 6)	J = 1	19 167.05
	3	←		2	19 279.45
	4	←		3	19 423.08
	5	←		4	19 525.34
$J^1\Pi_g^-$ (v' = 2)	3	←	$B^1\Sigma_u^+$ (v = 6)	3	19 193.04

Table II Term values (cm^{-1})[a] of $EF^1\Sigma_g^+$, $H^1\Sigma_g^+$, $I^1\Pi_g^+$, $J^1\Delta_g$ states

	$EF^1\Sigma_g^+$ (v' = 24)	$EF^1\Sigma_g^+$ (v' = 25)	$EF^1\Sigma_g^+$ (v' = 26)
J' = 0	.....	115 563.70[b]	116 041.59[b]
1	.....	115 577.75 (115 577.68)	116 031.71 (116 031.65)
2	115 079.95[b]	115 606.69 (115 606.77)	116 047.35 (116 047.33)
3	115 131.12[b]	115 653.88 (115 653.92)	116 088.66 (116 088.60)
4	115 207.34[b]	115 692.88[b]	116 151.58 (116 151.54)
5	115 275.77[b]	115 777.68[b]	116 232.43 (116 232.41)
	$EF^1\Sigma_g^+$ (v' = 27)	$EF^1\Sigma_g^+$ (v' = 28)	$EF^1\Sigma_g^+$ (v' = 29)
J' = 0	116 508.24[b]	116 915.36 (116 915.41)	.....
1	116 523.55[b]	116 931.85 (116 931.86)	.....
2	116 554.55[b]	116 964.41 (116 964.40)	117 391.57[b]
3	116 604.10[b]	117 016.23 (117 016.19)	.....
4	116 633.51[b]	117 068.80[b]	117 499.57[b]
5	116 721.99[b]	117 148.71[b]	117 576.95[b]
	$H^1\Sigma_g^+$ (v' = 1)	$H^1\Sigma_g^+$ (v' = 2)	
J' = 0	(115 251.52)	117 297.02 (117 297.09)	
1	(115 296.88)	117 338.53 (117 338.50)	
2	(115 393.84)	(117 455.50)	
3	(115 544.94)	(117 590.25)	
4	115 777.13[b]	(117 836.26)	
5	116 034.92[b]	(118 106.46)	
	$I^1\Pi_g^+$ (v' = 2)		
J'= 1	(116 103.65)		
2	116 148.32 (116 148.36)		
3	(116 214.23)		
4	(116 305.38)		
5	(116 883.64)		
	$J^1\Delta_g^+$ (v' = 2)	$J^1\Delta_g^-$ (v' = 2)	
J' = 2	116 787.69 (116 787.75)	(116 787.20)	
3	116 960.12 (116 960.16)	116 963.16 (116 963.17[c])	
4	117 193.20[b]	(117 191.62)	
5	117 413.90[b]	.....	

a. Obtained by adding the probe transition frequencies (Table I) to the corresponding term values of the $B^1\Sigma_g^+$ (v = 6, J) levels.
b. Previously unobserved terms.
c. Obtained by adding 8.01 cm^{-1} to Dieke's value[2].
Data in parenthesis are taken from Reference 11.

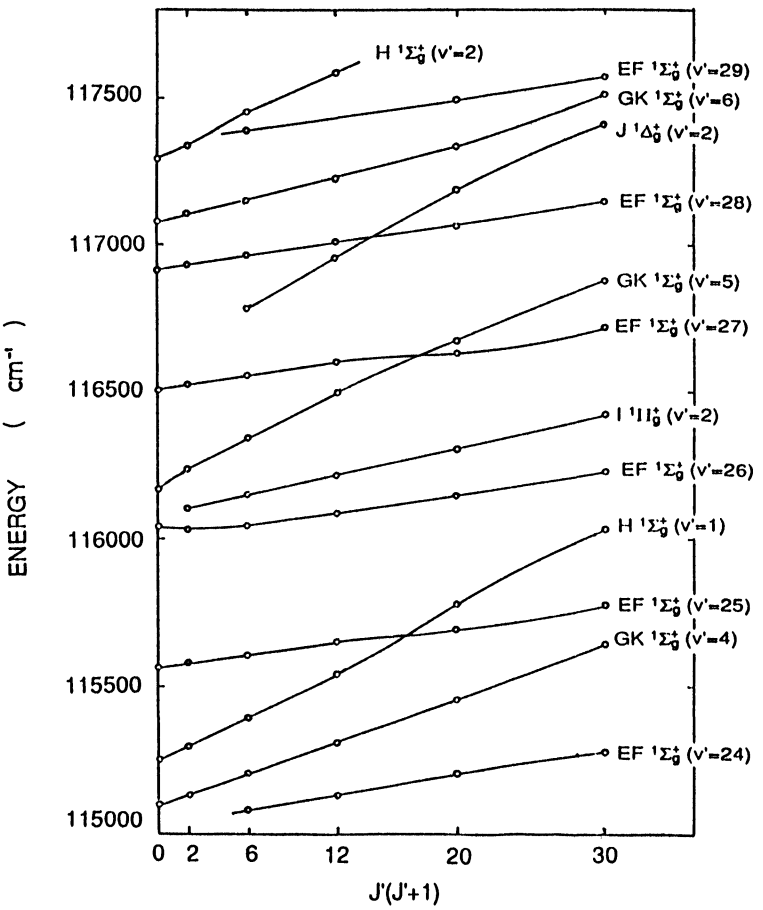

Figure 2 Plots of terms values T(v', J') vs J' (J' + 1).

III.2. Fluorescence lifetimes

The typical waveform of the fluorescence decay is illustrated in Figure 3, where open circles and solid line represent the experimental data and a single exponential fit to the data, respectively. Table III summarizes fluorescence lifetimes of the $EF^1\Sigma_g^+$ (v' = 24 ~ 29) and $J^1\Delta_g^+$ (v' = 2) states determined in the present work. Figures 4 (a) ~ 4 (c) display the plots of the experimental lifetimes against J'. The listed values are the averages of 3 to 12 measurements and the errors denote one standard deviations. The previous experimental values τ_{CDV} by Chien, Dalby, and Van der Linde[29] were derived from Hanle effect measurements. Two sets of theoretical values τ_{QDW1} and τ_{QDW2} by Quadrelli, Dressler, and Wolniewicz[11,12] represent results of the *ab initio* calculations. The former (τ_{QDW1}) takes the nonadi abatic coupling among the EF + GK + $H^1\Sigma_g^+$, $I^1\Pi_g$, and $J^1\Delta_g$ states into consideration. In addition, the

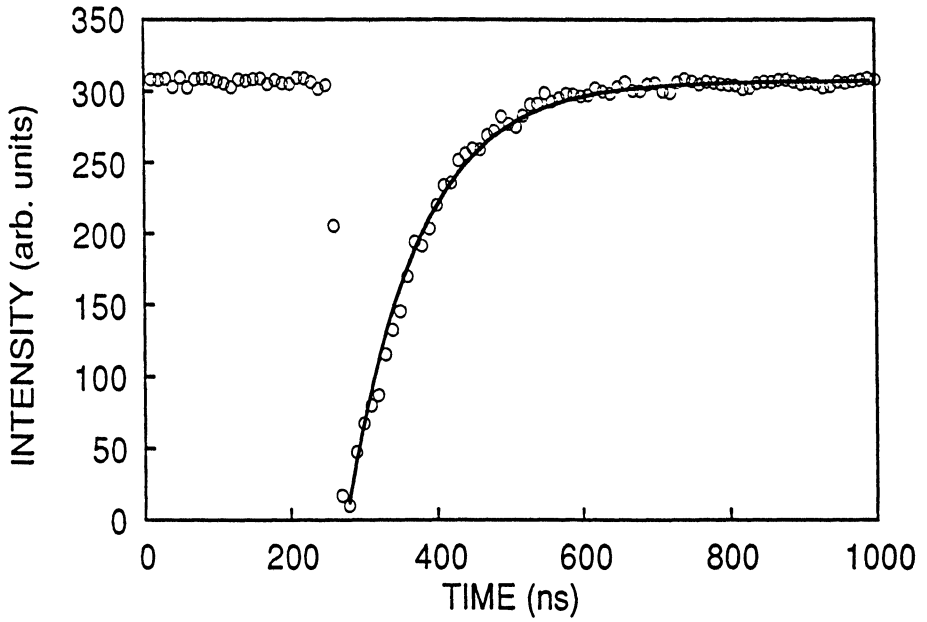

Figure 3 Time profile of the fluorescence decay in the $EF^1\Sigma_g^+$ ($v' = 28$, $J' = 3$) state. Single-exponential fit to the data is shown as a solid line.

predissociation induced by the nonadiabatic coupling with the ground state is taken into account in the latter (τ_{QDW2}). Therefore, τ_{QDW2} is smaller than τ_{QDW1}.

We evaluated the calculated radiative lifetimes τ_{calc} for $J' = 0 \sim 5$ after the procedure developed by Quadrelli et al.[11]. We employed, however, the simplified nonadiabatic wave functions consisting of only three adiabatic wavefunctions as listed in Table IV, while Quadrelli et al. employed the more complete nonadiabatic eigenvectors. For details the reader should refer to Reference 24. For the high vibrational levels of the $EF^1\Sigma_g^+$ state studied in the present work, the values of τ_{calc} are much longer than τ_{QDW1}. For example, $\tau_{QDW1} = 216$ ns and $\tau_{calc} = 560$ ns for $EF^1\Sigma_g^+$ ($v' = 26$, $J' = 0$). This discrepancy can be attributed to the above-mentioned simplification. In the high vibrational levels there might be greater contributions of the short-lived states such as the GK (for $J' \geq 0$), I (for $J' \geq 1$), and J (for $J' \geq 2$) adiabatic states.

The excited singlet *gerade* states lie above the H(1s) + H(1s) dissociation limit of the ground state and therefore become predissociative through the interaction with the dissociation continuum. Recently, Quadrelli et al.[12] discussed the predissociation of the first three excited $EF^1\Sigma_g^+$, $GK^1\Sigma_g^+$, and $H^1\Sigma_g^+$ states lying below H(1s) + H(2s, 2p) dissociation limit.

The predissociation probabilities P of the vibronic states were summarized in Table III of Reference 12. They vary over six orders of magnitude. For example, P is 2.86 s^{-1} for $EF^1\Sigma_g^+$ ($v' = 0$, $J' = 0$) and 1.89×10^6 s^{-1} for $EF^1\Sigma_g^+$ ($v' = 25$, $J' = 0$).

Table III Fluorescence lifetimes (ns) of $EF^1\Sigma_g^+$ and $J^1\Delta_g^+$ states

Nonadiabatic states	τ_{exp}[a]	τ_{CDV}[b]	τ_{QDW1}[c]	τ_{QDW2}[d]	τ_{calc}[e]
$EF^1\Sigma_g^+$ (v′ = 25)					
J′ = 0	260.8 ± 17.8		206	148	
1	257.1 ± 23.8		197	143	
2	248.8 ± 8.9				
3	188.8 ± 15.2				
4	238.7 ± 11.5				
$EF^1\Sigma_g^+$ (v′ = 26)					
J′ = 0	146.0 ± 11.5		216	164	
1	36.1 ± 0.5	48.5 ± 3.0	38.9	36.8	
2	46.1 ± 1.4				
3	54.9 ± 0.9				
4	59.6 ± 1.5				
$EF^1\Sigma_g^+$ (v′ = 27)					
J′ = 0	258.6 ± 24.0		275	227	
1	253.9 ± 15.2		255	213	
2	231.5 ± 9.7				
3	146.8 ± 3.3				
4	138.4 ± 1.9				
$EF^1\Sigma_g^+$ (v′ = 28)					
J′ = 0	115.0 ± 21.4		129	124	
1	108.5 ± 2.5		133	128	
2	115.8 ± 7.8				
3	95.5 ± 3.4				
4	115.8 ± 10.3				
$J^1\Delta_g^+$ (v′ = 2)					
J′ = 2	24.1 ± 1.4				28.1
3	27.5 ± 0.4				27.9
4	28.2 ± 0.1				25.7
5	39.1 ± 1.4				44.2

a. This work
b. Taken from Chien et al.[29]
c. Taken from Quadrelli et al.[11]
d. Taken from Quadrelli et al.[12]
e. Calculated values. See text for detail.

It is interesting to compare the total radiative decay rate A[11] with the nonradiative decay rate P for various vibrational states. For the $EF^1\Sigma_g^+$ (v′ = 19, 20, and 21) states, nonradiative decay probability is calculated to be at most 6% of the radiative one. On the other hand, the $EF^1\Sigma_g^+$ (v′ = 25 and 26) states have considerably large nonradiative probabilities: the ratio P/(A + P) reaches 28% and 24%, respectively. τ_{QDW2} in Table III corresponds to the calculated lifetimes of $\tau = 1/(A + P)$. Total decay rates of J′ = 1 levels are computed with combining the radiative decay rates for

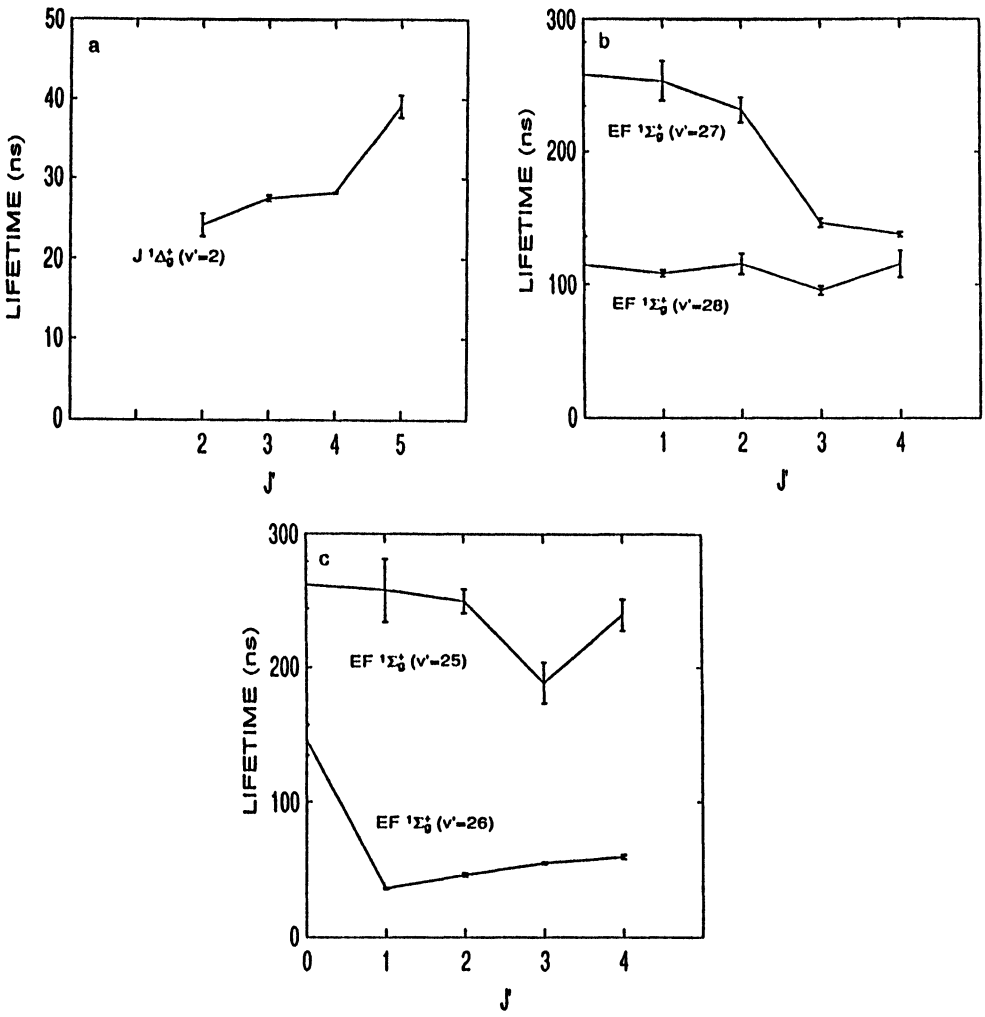

Figure 4 Plots of fluorescence lifetimes (τ_{exp}) vs J'.
a) The $J^1\Delta_g^+$ (v' = 2) state.
b) The $EF^1\Sigma_g^+$ (v' = 28) and the $EF^1\Sigma_g^+$ (v' = 27) states.
c) The $EF^1\Sigma_g^+$ (v' = 26) and the $EF^1\Sigma_g^+$ (v' = 25) states.

J' = 1 with the nonradiative rates calculated for J' = 0. The radiative decay rates of J' = 1 levels can significantly differ from those of J' = 0 levels in case that the vibronic states are coupled with the $I^1\Pi_g$ state. On the other hand, the J dependence of the nonradiative rates can be assumed to be considerably smaller, because the predissociation of the J' = 0 and 1 levels is governed entirely by the homogeneous $^1\Sigma_g^+ - {}^1\Sigma_g^+$ interaction; the heterogeneous $I^1\Pi_g - X^1\Sigma_g^+$ interaction does not contribute significantly to the predissociation of the J' = 1 levels.

Table IV The nonadiabatic wave function Ψ on the basis of vibronic adiabatic wave function ψ taken from Reference 11.

Ψ(EF25, J′ = 0) =	0.93859 ψ(EF25)	+0.23711 ψ(GK4)	–0.12604 ψ(GK5)
Ψ(EF25, J′ = 1) =	0.93507 ψ(EF25)	+0.23410 ψ(GK4)	–0.13029 ψ(GK5)
Ψ(EF25, J′ = 2) =	0.92660 ψ(EF25)	+0.23353 ψ(GK4)	–0.13493 ψ(GK5)
Ψ(EF25, J′ = 3) =	0.88333 ψ(EF25)	–0.28539 ψ(H1)	+0.25505 ψ(GK4)
Ψ(EF25, J′ = 4) =	0.89386 ψ(EF25)	+0.31163 ψ(H1)	–0.14913 ψ(GK5)
Ψ(EF26, J′ = 0) =	0.94161 ψ(EF26)	+0.18046 ψ(GK5)	+0.14554 ψ(EF25)
Ψ(EF26, J′ = 1) =	0.71741 ψ(EF26)	–0.55999 ψ(I2)	+0.31823 ψ(GK5)
Ψ(EF26, J′ = 2) =	0.72859 ψ(EF26)	–0.49711 ψ(I2)	+0.35964 ψ(GK5)
Ψ(EF26, J′ = 3) =	0.77699 ψ(EF26)	–0.41037 ψ(I2)	+0.34907 ψ(GK5)
Ψ(EF26, J′ = 4) =	0.82842 ψ(EF26)	–0.32784 ψ(I2)	+0.31205 ψ(GK5)
Ψ(EF27, J′ = 0) =	0.94086 ψ(EF27)	+0.18300 ψ(GK6)	+0.16794 ψ(EF26)
Ψ(EF27, J′ = 1) =	0.94054 ψ(EF27)	+0.17771 ψ(GK6)	+0.16441 ψ(EF26)
Ψ(EF27, J′ = 2) =	0.93687 ψ(EF27)	+0.16359 ψ(GK6)	+0.15638 ψ(EF26)
Ψ(EF27, J′ = 3) =	0.90333 ψ(EF27)	–0.23670 ψ(I2)	–0.20096 ψ(GK5)
Ψ(EF27, J′ = 4) =	0.77919 ψ(EF27)	+0.43577 ψ(GK5)	+0.26318 ψ(I2)
Ψ(EF28, J′ = 0) =	0.85174 ψ(EF28)	–0.36625 ψ(GK6)	+0.24174 ψ(EF27)
Ψ(EF28, J′ = 1) =	0.85984 ψ(EF28)	–0.35124 ψ(GK6)	+0.23705 ψ(EF27)
Ψ(EF28, J′ = 2) =	0.87354 ψ(EF28)	–0.32172 ψ(GK6)	+0.22653 ψ(EF27)
Ψ(EF28, J′ = 3) =	0.87549 ψ(EF28)	–0.26265 ψ(GK6)	+0.19907 ψ(EF27)
Ψ(EF28, J′ = 4) =	0.88778 ψ(EF28)	–0.23780 ψ(GK6)	+0.21689 ψ(J2)
Ψ(J2, J′ = 2) =	0.98172 ψ(J2)	–0.17493 ψ(I2)	–0.04255 ψ(I3)
Ψ(J2, J′ = 3) =	0.94282 ψ(J2)	–0.23326 ψ(I2)	+0.16859 ψ(EF28)
Ψ(J2, J′ = 4) =	0.90729 ψ(J2)	–0.31249 ψ(I2)	–0.21293 ψ(EF28)
Ψ(J2, J′ = 5) =	0.71996 ψ(J2)	–0.52454 ψ(GK6)	–0.28863 ψ(EF29)

In the following, the collision-free fluorescence lifetime is compared with the theoretical lifetime by Dressler and co-workers[11,12] for each of the rovibronic levels in the $J^1\Delta_g^+$ (v′ = 2) and $EF^1\Sigma_g^+$ = (v′ = 25 ~ 28) states.

The $J^1\Delta_g^+$ (v′ = 2) state

The fluorescence lifetimes for the $J^1\Delta_g^+$ (v′ = 2) state are measured to be 25 ~ 40 ns. The J′ = 5 level has a longer fluorescence lifetime than the other rotational levels. This is explained by the fact that the $J^1\Delta_g^+$ (v′ = 2, J′ = 5) nonadiabatic wave function has appreciable contributions from the long-lived GK (v = 6) (τ_{GK6} = 47 ns) and EF (v = 29) (τ_{EF29} = 772 ns) adiabatic states as seen in Table IV. τ_{calc} for J′ = 2 ~ 5 levels are given in Table III to supplement the data by Quadrelli et al.[11] As in our previous study,[24] the value of 4×10^7 s^{-1} was assumed for the transition probability $A(^1\Delta_g)$ of the noninteracting $J^1\Delta_g^+$ state. The agreement between τ_{exp} and τ_{calc} is excellent, implying that the adiabatic lifetime of the $J^1\Delta_g^+$ state depends little on the vibrational state.

The $EF^1\Sigma_g^+$ (v′ = 28) state

Concerning the $EF^1\Sigma_g^+$ (v′ = 28) state, any appreciable rotational dependence of the lifetimes is not observed. The effect of the short-lived J (v = 2) adiabatic state to

the $J' = 4$ level expected from Table IV is not apparent. The agreement between our values and τ_{QWD1} seems reasonable.

The $EF^1\Sigma_g^+$ ($v' = 27$) state

The fluorescence lifetimes for the $EF^1\Sigma_g^+$ ($v' = 27$) state show a considerable J' dependence. The shorter lifetimes observed for the $J' = 3$ and 4 levels are consistent with the nonadiabatic wave functions coupled with the short-lived I ($v = 2$) adiabatic state. The experimental lifetimes for the $EF^1\Sigma_g^+$ ($v' = 27$, $J' = 0$ and 1) levels agree better with τ_{QDW1} than with τ_{QDW2}.

The $EF^1\Sigma_g^+$ ($v' = 26$) state

A remarkable rotational dependence of τ_{exp} is observed for the $EF^1\Sigma_g^+$ ($v' = 26$) state. The short lifetimes of the $J' = 1 \sim 4$ levels are ascribed to the large contributions of the I ($v = 2$) adiabatic state to their nonadiabatic wave functions. This strong interaction for $J' \geq 1$ levels is understood qualitatively by the fact that the $EF^1\Sigma_g^+$ ($v' = 26$) and $I^1\Pi_g^+$ ($v' = 2$) states are located nearby each other as seen in Figure 2. The repulsion between $J' = 1$ levels shifts the $EF^1\Sigma_g^+$ ($v' = 26$, $J' = 1$) level downward to below $J' = 0$ as already mentioned in III.1. Chien et al.[29] have obtained somewhat longer lifetime ($\tau_{CDV} = 48.5 \pm 3.0$ ns) for $J' = 1$ level than our value. Their value was derived from the Hanle effect measurements without correcting for the hyperfine effects.

The $EF^1\Sigma_g^+$ ($v' = 26$ and also 25) states have large nonradiative decay rates. Consequently, τ_{QDW2} is calculated to be considerably shorter than τ_{QDW1}. Therefore, τ_{QDW2} reproduces our experimental fluorescence lifetime for the $EF^1\Sigma_g^+$ ($v' = 26$, $J' = 0$) level much better than τ_{QDW1}.

The $EF^1\Sigma_g^+$ ($v' = 25$) state

The lifetime for the $EF^1\Sigma_g^+$ ($v' = 25$, $J' = 3$) is much shorter than those for other J', although a notable rotational dependence of the lifetimes is not expected from their nonadiabatic wavefunctions listed in Table IV. The lifetimes measured at $J' = 0$ and 1 levels are ~30% longer than the values of τ_{QDW1}. For a more precise comparison the following two factors must be taken into account as mentioned by Quadrelli et al.[11]:

(i) The neglect of the nonadiabatic couplings with the higher electronic states derived from the *ns* and *nd Rydberg series* and from the doubly excited $^1\Sigma_g^+$ configurations.
(ii) The remaining convergence errors in the calculations of the clamped-nuclei electronic energies.

Acknowledgement

This work was partly supported by a Special Grant for Promotion of Research from RIKEN.

References

1. O. W. Richardson, Molecular Hydrogen and its spectrum (Yale University, New Haven, Connecticut 1934).
2. G. H. Dieke. *J. Mol. Spectrosc.*, **2**, 494 (1958).
3. H. M. Crosswhite, The Hydrogen Molecule Wavelength Tables of GerhardHeinrich Dieke (Wiley-Interscience, New York 1972).
4. E. R. Davidson. *J. Chem. Phys.*, **33**, 1577 (1960).
5. E. D. Davidson. *J. Chem. Phys.*, **35**, 1189 (1961).
6. K. Dressler, R. Gallusser, P. Quadrelli and L. Woleniewicz. *J. Mol. Spectorsc.*, **75**, 205 (1979).
7. M. Glass-Maujean, P. Quadrelli, K. Dressler and L. Woleniewicz. *Phys. Rev.*, **A28**, 2868 (1983).
8. M. Glass-Maujean, P. Quadrelli, and K. Dressler. *At. Data Nucl. Data Tables* **30**, 273 (1984).
9. M. Glass-Maujean, P. Quadrelli and K. Dressler. *J. Chem. Phys.*, **80**, 4355 (1984).
10. P. Senn, and K. Dressler. *J. Chem. Phys.*, **87**, 6908 (1987).
11. P. Quadrelli, K. Dressler, and L. Woleniewicz. *J. Chem. Phys.*, **92**, 7461 (1990) (AIP document No. PAPS JCPSA-92-7461-59).
12. P. Quadrelli, K. Dressler, and L. Woleniewicz. *J. Chem. Phys.*, **93**, 4958 (1990).
13. P. Chahill. *J. Opt. Soc. Am.*, **59**, 875 (1969).
14. R. J. Anderson, J. Watson and F. A. Sharpton. *J. Chem. Phys.*, **67**, 1641 (1977).
15. R. D. Day, R. J. Anderson and F. A. Sharpton. *J. Chem. Phys.*, **71**, 3683 (1979).
16. N. Böse and F. Linden. *J. Phys.*, **B14**, 2499 (1981).
17. C. Gómez-Reino and J. Campos. *An. Fis.*, **72**, 219 (1976).
18. J. A. Sanchez and J. Campos. *J. Phys.*, (France) **49**, 445 (1988).
19. D. J. Kligler and C. K. Rhodes. *Phys. Rev. Lett.*, **40**, 309 (1978).
20. N. Bjerre, R. Kachru and H. Helm. *Phys. Rev.*, **A31**, 1026 (1985).
21. E. E. Marinero, C. T. Rettner and R. W. Zare. *Phys. Rev. Lett.*, **48**, 1323 (1982).
22. E. E. Marinero, R. Vasudev and R. N. Zare. *J. Chem. Phys.*, **78**, 692 (1983).
23. D. W. Chandler and L. R. Thorne. *J. Chem. Phys.*, **85**, 1733 (1986).
24. K. Tsukiyama, J. Ishii and T. Kasuya. *J. Chem. Phys.*, **97**, 875 (1992).
25. K. Tsukiyama, S. Shimizu and T. Kasuya. *J. Mol. Spectrosc.*, **155**, 352 (1992).
26. H. Rottke and K. H. Welge. *J. Chem. Phys.*, **97**, 908 (1992).
27. I. Dabrowski. *Can. J. Phys.*, **62**, 1639 (1984).
28. L. Wolniewicz and K. Dressler. *J. Mol. Spectrosc.*, **67**, 416 (1977).
29. C. W. Chien, F. W. Dalby and J. Van der Linde. *Can. J. Phys.*, **56**, 827 (1978).